Current Biology *17*, 12–19, January 9, 2007 DOI 10.1016/j.cub.2006.11.027

Article

The Chemotactic Behavior of Computer-Based Surrogate Bacteria

Dennis Bray,[1,*] Matthew D. Levin,[1] and Karen Lipkow[1]
[1] Department of Physiology, Development, and Neuroscience
University of Cambridge
Downing Street
Cambridge CB2 3DY
United Kingdom

Summary

Background: Chemotaxis is the process by which organisms migrate toward nutrients and favorable environments and away from toxins and unfavorable environments. In many species of bacteria, this occurs when extracellular signals are detected by transmembrane receptors and relayed to flagellar motors, which control the cell's swimming behavior.
Results: We used a molecularly detailed reaction-kinetics model of the chemotaxis pathway in *Escherichia coli* coupled to a graphical display based on known swimming parameters to simulate the responses of bacteria to 2D gradients of attractants. The program gives the correct phenotype of over 60 mutants in which chemotaxis-pathway components are deleted or overexpressed and accurately reproduces the responses to pulses and step increases of attractant. In order to match the known sensitivity of bacteria to low concentrations of attractant, we had to introduce a set of "infectivity" reactions based on cooperative interactions between neighboring chemotaxis receptors in the membrane. In order to match the impulse response to a brief stimulus and to achieve an effective accumulation in a gradient, we also had to increase the activities of the adaptational enzymes CheR and CheB at least an order of magnitude greater than published values. Our simulations reveal that cells develop characteristic levels of receptor methylation and swimming behavior at different positions along a gradient. They also predict a distinctive "volcano" profile in some gradients, with peaks of cell density at intermediate concentrations of attractant.
Conclusions: Our results display the potential use of computer-based bacteria as experimental objects for exploring subtleties of chemotactic behavior.

Introduction

The intracellular reactions by which coliform bacteria detect and respond to attractants and repellents form the basis of probably the simplest known behavioral response (Figure 1) [1, 2]. A handful of receptor species in the membrane detect environmental signals and relay this information to a single intracellular kinase, CheA, which changes its rate of generation of phosphoryl groups. Phosphoryl groups are transferred from the kinase to a small highly mobile protein, CheY, which then diffuses to the flagellar motors. The motors change their direction of rotation depending on the local concentration of phosphorylated CheY (CheYp) and thereby modify the pattern of swimming of the bacterium. Two other enzymes mediate adaptation—a simple form of cellular "memory": One enzyme (CheR) adds methyl groups to the receptors and the other (CheB) removes them. All of the proteins in this pathway, from input to output, have been identified, purified, and studied in vitro, and we have atomic level structures for all of them, in whole or in part. Systematic mutagenesis confirms that we have essentially all the players in the pathway and also provides a rich database of phenotypes. Sophisticated optical methods allow the activities and concentrations of certain signaling components to be measured, even in single cells. Several computer models of the signaling process have been developed and show broad agreement with experimental data (see http://www.pdn.cam.ac.uk/comp-cell/Models.html).

The sensitivity of the chemotactic response, particularly to aspartate, has been the subject of great interest. *E. coli* bacteria can detect a change in occupancy of their aspartate receptors (Tar) of as little as 0.1%–0.2%, corresponding to the binding of a few molecules per cell [3]. However, predictions based on the canonical signaling cascade and embodied in early computer models consistently failed to reproduce anything like this amplification (also known as "gain")—in most cases, there is a missing amplification of about 30-fold [4, 5]. Present evidence suggests that this arises from the neighboring receptors' cooperative interactions, facilitated by the tendency of receptors and their associated signaling molecules to cluster on the bacterial surface [6]. Although the mechanistic details remain a matter of debate, it is now generally accepted that influences spreading from occupied receptors to neighboring unoccupied receptors substantially increase the size of the downstream signal [7].

Biochemical changes in the chemotaxis pathway are context specific and make sense only when one knows the chemical environment of the bacterium. A complete description therefore requires one to relate *temporal* changes in the concentrations of signaling molecules to *spatial* changes in attractants and repellents. With this in mind, we embedded a detailed, quantitative simulation of the temporal changes in chemotaxis biochemical reactions within a graphical representation of swimming bacteria. In the resulting program, individual bacteria are displayed running (swimming smoothly in an approximately constant direction) and tumbling (with little change in position) within a 2D terrain, with more or less accurate detail, depending on the magnification scale. The terrain includes a user-specified gradient of attractant (in this case aspartate) sampled by the bacterium at regular intervals (typically four times per s). For the simulations described in this paper, a single attractant—aspartate—and only one receptor type, Tar,

*Correspondence: db10009@cam.ac.uk

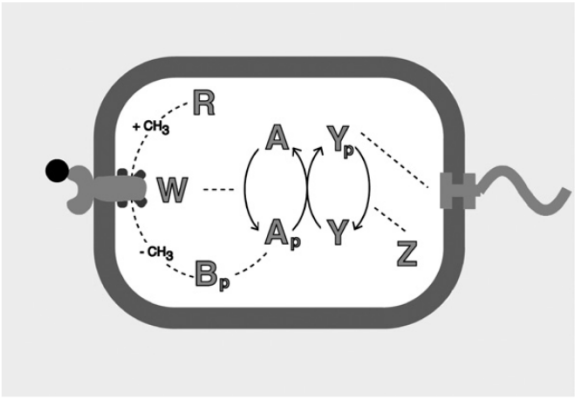

Figure 1. The *E. coli* Chemotaxis Pathway

A schematic of the cell shows the signaling proteins (letters R, B, W, A, Y, and Z represent the proteins CheR, CheB, CheW, CheA, CheY, and CheZ) that carry signals from transmembrane receptors (left) to flagellar motors (right). See recent reviews by [2], [7], and [26].

was used. Instantaneous changes in extracellular aspartate due to the motion of the bacterium result in rapid shifts in the concentrations of phosphorylated protein species and slower modulation of the levels of protein methylation. Random number generators in the program then convert the instantaneous concentration of the intracellular signal to a probability of tumbling. Each tumble then produces a random change in swimming direction based on experimentally observed parameters [8].

The simulated bacterium thus pursues a biased random walk over the computer screen in a manner responsive to the local concentrations of aspartate. At any instant of time, one can read out the concentrations of extracellular aspartate and intracellular signaling molecules in an individual bacterium as well as other parameters such as the rotational bias of the flagellar motor. The same approach can be applied to populations of bacteria, revealing their changing distribution with time. Evidently, these simulations have many obvious differences to real bacteria, as we discuss below. Nevertheless, the virtual bacteria reproduce a broad range of experimental data relating to the sensitivity and rates of response and adaptation, for both wild-type cells and chemotactic mutants. Because their internal biochemistry is firmly based on decades of experimental data, we believe it is legitimate to treat these representations as experimental objects in their own right. The advantage is that we can expose cells of any specified genotype to precisely defined stable gradients of any required shape (including those that are difficult, or impossible, to achieve in the real world) and observe their behavioral responses.

Results

Two graphical representations, termed *E. solo* and *E. pluribus*, were prepared for this study. Both are based on a compact version of an existing program BCT (Bacterial ChemoTaxis) (see Experimental Procedures). In the *E. solo* program, one or a few bacteria are depicted at relatively high magnification, with each cell having four independent flagella. Here, the environment contains a uniform concentration of aspartate, which can be adjusted in real time by the user. This program allows the analysis of such details as the frequency of tumbles and angles of turns during a tumble, adaptation times, and the small changes in direction during a run due to thermal motion. In the program called *E. pluribus*, bacteria are represented at lower magnification and without flagella. In this case, multiple bacteria (of the same or different genotype) are allowed to swim within a defined arena, rectangular or circular, containing a fixed gradient of aspartate of specified slope. Bacteria that happen to swim into the arena boundaries either bounce back into the arena (reflective boundary) or pass through and reappear on the opposite side of the arena (toroidal boundary).

Figure 2 depicts a series of snapshots of a single bacterium taken from the *E. solo* program at roughly 1 s intervals. The bacterium is seen swimming across the computer screen with occasional tumbles. The four flagella are either coordinated into a single sinusoidal bundle during a run or splayed apart during a tumble. Experimental records of swimming bacteria [9] are shown in Figures 3A–3C, where they are compared to the loci of individual *E. solo* from the simulation (Figures 3D–3F). Tracks include both wild-type bacteria and a mutant that does not tumble. In the simulated case (Figure 3F), the mutant is one in which all of the signal transduction proteins were removed except CheA—these cells fail to make the phosphorylated protein CheYp and therefore display exclusively smooth swimming. Figures 3G and 3H provides a comparison of the durations of runs and tumbles measured in tethered cells and taken from the *E. solo* simulation (with input data taken from the experimental distributions).

Many other mutants in the chemotaxis pathway have been isolated and characterized in over four decades of research. These include mutants in which the signal transduction genes have been deleted, singly or in combination, mutants in which genes are expressed at higher than normal levels, usually through the introduction of a plasmid, and mutants in which all of the signal transduction genes have been removed by deletion (a "gutted" strain) and then selected genes replaced. Each mutant exhibits a characteristic defect in its chemotactic ability. Absence of the phosphatase CheZ, for example, results in the accumulation of CheYp and thus leads to tumbly behavior and a prolonged response to transient stimuli. A smooth-swimming phenotype is exhibited not only by mutants lacking the adaptor protein CheW but also by those in which it is overexpressed, a pattern thought to reflect the optimum combinations of proteins for building the receptor complex [10]. These and other patterns are reproduced by the BCT program, which gives qualitative agreement with the phenotypes of 63 out of 65 mutants (Table 1). Whether the few remaining discrepancies on this list are significant remains to be explored.

In response to a step increase in aspartate concentration, the swimming performance of *E. solo* changes abruptly. The counterclockwise swimming bias rises rapidly from around 0.85 [9, 11] to a value closer to 1.0, indicating a suppression of tumbles. Note that this unstimulated bias is a population average with the individual bias varying from cell to cell [12], although greater

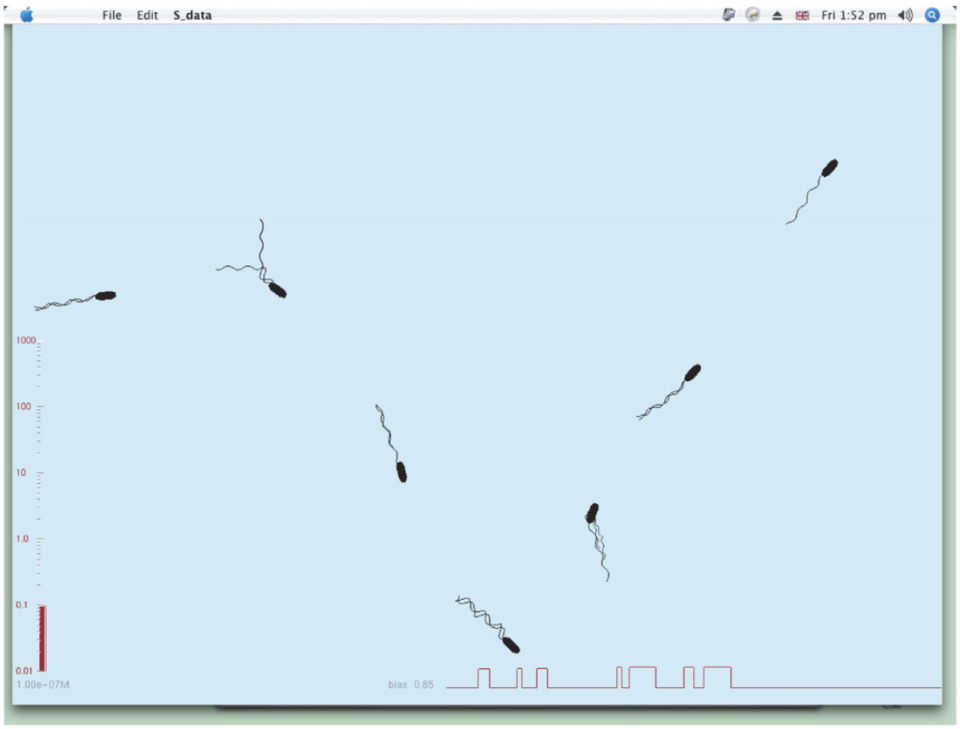

Figure 2. Simulated Swimming Bacteria

Screen shots of a simulated *E. coli* bacterium generated by the *E. solo* program, in which the bacterium is running and tumbling in a uniform background of 0.1 μM aspartate. The bacterium has four flagella, which either combine into a regular bundle in a run or break apart individually during tumbles. The local concentration of aspartate is given on the left-hand scale; steps in the lower trace represent tumble events. The dimensions of the terrain are 110 × 80 μm, and the snapshots are taken at 1 s intervals.

sensitivity is achieved with biases closer to 0.5. The bias then slowly falls over a period of seconds or minutes because of the adaptation of the system. Analysis of the *E. solo* signaling intermediates reveals a progressive increase in the level of receptor methylation as adaptation proceeds (data not shown). If aspartate is suddenly removed from a fully adapted *E. solo*, the bias rapidly falls and is followed by a slow return of the bias and the methylation level to their default unstimulated values.

A similar but more rapid sequence of events is seen when *E. solo* is exposed to a rapid pulse of aspartate (Figure 4). The magnitude of the attractant response (the peak value reached) varies monotonically with the aspartate concentration encountered, within its effective range, and depends on the sensitivity or gain of the system, already mentioned. In order to achieve a suitable sensitivity in the BCT program (which does not represent individual receptor molecules), we introduced an "infectivity" factor as an input to the program. This amplifies the effect of aspartate binding and thereby approximates the source of gain in the system. The basis of the infectivity calculation was presented previously [13]. Each inactive (occupied) receptor complex causes a number of active neighboring complexes to become inactive depending on the infectivity and present level of occupancy. In Figure 4, we show simulated step and impulse responses with an infectivity of 35, based on the enhancement in sensitivity exhibited by wild-type cells over *cheRcheB* mutants [5]. With an infectivity of this magnitude and pulses of aspartate that reach the experimentally recorded maximal bias, we found it necessary to increase the activities of CheR and CheB—the two enzymes responsible for adaptation—15-fold to match the time courses of the two responses.

Infectivity and rate of adaptation both influence the ability of simulated bacteria to accumulate in a gradient. This was examined with the *E. pluribus* simulation of cells in a radial gradient. In an exponential aspartate gradient, 10^{-5} M at the center and 10^{-9} M on the perimeter, default *E. pluribus* cells (which have an infectivity of 1) show very little tendency to accumulate (Figure 5A). Cells with an infectivity of 35 in the same gradient show a peak of density at approximately 6×10^{-8} M (Figure 5B). Note that this peak of cell density does not coincide with the maximum aspartate concentration. A 15-fold increase in the activities of adaptational enzymes CheR and CheB caused the distribution to shift closer to the center of the gradient (Figure 5C) with a significant proportion of cells escaping the influence of the gradient. The tightest concentration of cells was seen when both CheR and CheB and infectivity were elevated (Figure 5D).

Screen shots of *E. pluribus* cells in a radial gradient taken after they have reached equilibrium are shown in Figure 6. In this case, the strain—with an increased CheR and CheB activity (15-fold)—was exposed to different gradients of aspartate. With a high peak concentration and steep gradient, the cells displayed a flattened central plateau (Figure 6B), which became sharper when the peak concentration was decreased (Figure 6C). As the gradient became less steep and the absolute

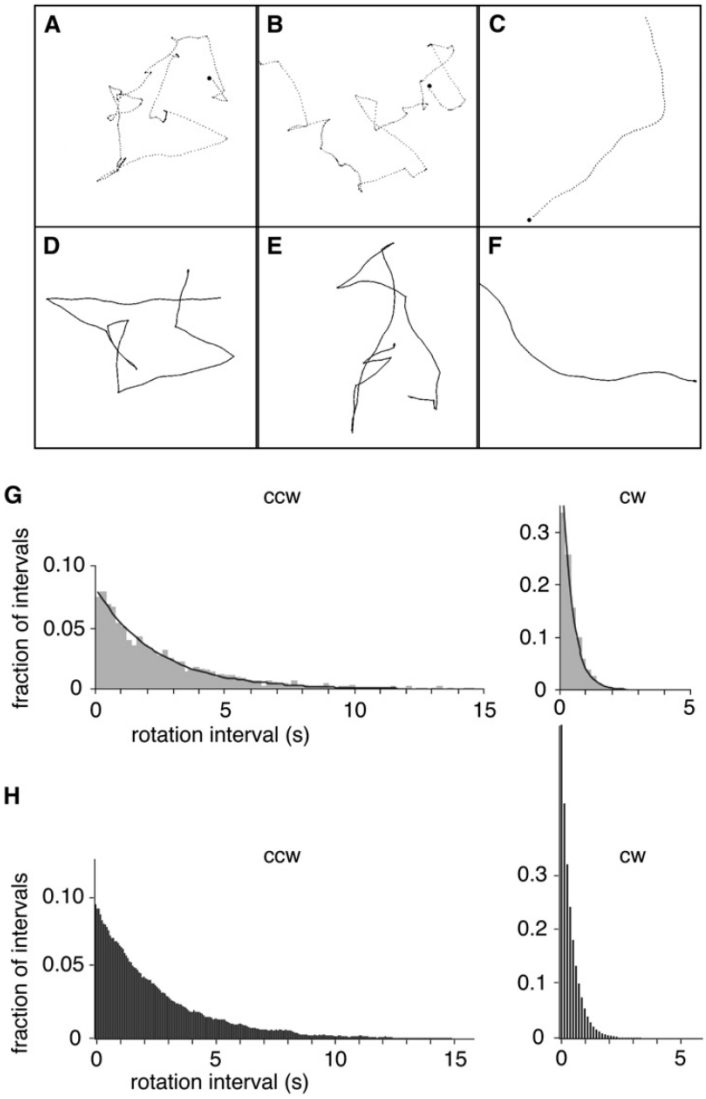

Figure 3. Swimming Characteristics of Real and Simulated Bacteria

Loci of bacteria recorded experimentally or generated by computer.

(A–C) Experimental data reproduced from Berg and Brown [9] (2D projection of 3D track).

(D–F) Simulations based on the *E. solo* program with graphical interface employing closely similar swimming speeds, spatial dimensions, and recording times.

(G) Distributions of lengths of "runs" (CCW) and "tumbles" (CW) obtained experimentally for wild-type cells tethered to a microscope slide by antibody. Reproduced from Morton-Firth [27].

(H) Equivalent distributions generated by computer.

concentrations became lower, increasing numbers of cells escaped its influence (Figure 6D).

In some radial gradients, especially those with high maximum attractant concentration, the cell population developed a distinctive "volcano" shape at steady state (Figure 7A and Figure S1). On closer examination, it appeared that under these conditions, the peak of cell density coincided with the location at which cells had the greatest probability of tumbling. Analysis of the cells in this situation shows that, in the central crater of the volcano, cells had a bias close to 1.0 and spent most of their time in a run. Systematic changes in methylation level of receptors were also noted from the lowest (default) level at the gradient perimeter to an elevated level closer to the center (Figure 7B).

Discussion

In this study, we embedded an established ordinary-differential equation model of the signaling reactions of the *E. coli* chemotaxis pathway into graphical displays of swimming bacteria. The resulting program permitted us to test the responses of the cells to their environment and, specifically, to examine how cells with different internal functionality behave in various gradients of attractants.

As in any computational analysis, we had to make simplifications, and many features of the real biological system were omitted. Thus, we encoded only the cascade of reactions between the chemotactic receptors and the flagellar motor and ignored all other aspects of cell chemistry. We did not include crosstalk with other signaling pathways, such as the PTS system for glucose, influences due to metabolism, or slower effects due to cell division or protein synthesis. Even the chemotaxis pathway itself was represented in a highly reduced and stripped-down format: Just one type of receptor was present (instead of five), and adaptation was achieved by addition of a single methyl group per receptor dimer (instead of eight). In contrast to other programs we have developed such as StochSim [14] and *Smoldyn* [15], the BCT program does not represent individual molecules explicitly nor does it specify where they are in the cell, whether they diffuse, and, if so, when they diffuse. Flagella and their associated motors were not modeled with any detail in our program (the display

Table 1. Chemotaxis Mutants[a]

Deletion	Gutted	Overexpression	Mixed
T^-	Gutted (g)	T^{++}	T^-B^{++}
R^-	Y^+ (g)	R^{++}	T^-Y^{++}
B^-	Y^{++} (g)	B^{++}	$T^{++}Z^-$
W^-	Y^{+++} (g)	W^{++}	B^-W^{++}
A^-	Y^{++++} (g)	A^{++}	B^-Z^{++}
Y^-	Z^t (g)	Y^{++}	$B^{++}Z^-$
Z^-	Y^+Z^t (g)	Z^{++}	$W^{++}Z^-$
T^-Z^-	$Y^{++}Z^t$ (g)	$T^{++}W^{++}$	$A^{++}Z^-$
R^-B^-	$Y^{+++}Z^t$ (g)	$B^{++}Y^{++}$	$T^-B^{++}Y^{++}$
B^-Z^-	$Y^{++++}Z^t$ (g)	$W^{++}A^{++}$	$T^-W^{++}Z^-$
W^-A^-	T^+Y^+ (g)	$Y^{++}Z^{++}$	$T^{++}W^-Z^-$
W^-Z^-	A^+Y^+ (g)		$R^-B^-W^{++}$
A^-Z^-	$T^+A^+Y^+$ (g)		$R^-B^-Y^{++}$
Y^-Z^-	$W^+A^+Y^+$ (g)		
$T^-W^-Z^-$	$T^+W^+A^+Y^+$ (g)		
$B^-W^-A^-$	$T^+Y^+Z^t$ (g)		
$B^-Y^-Z^-$	$A^+Y^+Z^t$ (g)		
$W^-A^-Z^-$	$T^+A^+Y^+Z^t$ (g)		
	$W^+A^+Y^+Z^t$ (g)		
	$T^+W^+A^+Y^+Z^t$ (g)		
	$T^{++}Y^{++}$ (g)		
	$W^+Y^+Z^t$ (g)		
	$T^+W^+Y^+Z^t$ (g)		

Gene products are either deleted (–), present at wild-type levels (+), increasingly overexpressed (++, +++, ++++), or present in trace amounts (t). The symbol (g) indicates expression in a gutted strain, in which all of the chemotaxis genes are deleted. BCT is able to reproduce the phenotypes of all mutants except those that are shaded. This list includes a set of gutted strains newly isolated because of differences they showed to the results of BCT simulations: The program in this case served to identify a flaw in the original genetic assignments [28].

[a] Genotypes of mutants whose phenotypes have been reported in the literature.

of flagella in *E. solo* simply imitates the appearance of flagella seen under a microscope and does not embody biophysical parameters). The probability of a run or tumble of each bacterium was calculated by a simple formula from the instantaneous concentration of CheYp. Gradients and swimming patterns were all rendered in 2D instead of the more natural 3D. The positions of bacteria were represented internally as dimensionless points, and no interactions, physical or otherwise, between different cells were considered.

Despite these approximations, and within the prescribed limits, our simulated bacteria closely resemble real cells. The durations of their runs and tumbles have the same distributions as those recorded for living cells and show the same angles of turn during a tumble. Their random drift during a run is comparable in magnitude to the effects of thermal motion seen in real cells. Steady-state swimming behavior of a large number of chemotactic mutants was qualitatively correct (Table 1), as were changes in run length caused by the attractant aspartate. Quantitative agreement was obtained after adjustment of gain and adaptation rate as described in the text. This applied to the response to a transient aspartate pulse, which showed the expected peak size and overshoot, as well as to the time course of adaptation (Figure 4). Once changes to the gain and adaptation time course had been installed, populations of simulated bacteria (*E. pluribus* simulation) effectively accumulated in simulated gradients.

In this work, because the BCT program represents receptors as concentrations rather than as individual molecules, we approximated the effects of receptor cooperation by including an "infectivity" term in our program. At low concentrations of attractant, this simply multiplies the receptor occupancy by a constant factor. At higher concentrations, the effect of aspartate plateaus due to overlap between neighboring receptors (the "raindrops effect" [13]). Increased infectivity had a marked effect on the rapid impulse response of bacteria and caused the peak bias to increase. An infectivity of approximately 35 was sufficient for generating a gain close to that seen experimentally. Increased infectivity also affected the distribution of bacteria in a gradient and moved the threshold accumulation to lower concentrations (compare Figures 5A and 5B).

We also found it necessary to modify the rate of adaptation. Experimental records of the impulse response show a biphasic time course, in which the bias first rises rapidly then falls transiently below the resting bias before returning to its initial state (see Figure 4C). The second phase, or "overshoot," was almost absent from the simulated transient response of default cells, even with increased gain (Figure 4D). However, we found that we were able to achieve an overshoot of the desired magnitude by increasing the kinetic rates of CheR and CheB, the two enzymes responsible for adaptation, 10- to 20-fold based on simulations of the step response (Figure 4A). Published estimates for the rate of demethylation of receptors are 0.4 per s for phosphorylated CheB [16] and an approximately 70-fold-lower rate for unphosphorylated CheB [17]. Experimental values for the rate of CheR methylation range from 2×10^{-4} per s to over 5×10^{-3} per s (see http://www.pdn.cam.ac.uk/comp-cell/Exp_data/edmeth.htm). In the present version of BCT, a higher rate of CheR (2.7×10^{-2} per s) is selected to produce a resting bias of 0.85 [9, 11]. As described in this paper, we found it necessary to increase the kinetic rates of CheR and CheB even further to achieve the impulse overshoot (Figure 4D) and effective accumulation in a gradient (Figure 5D). Note that all estimated values of catalytic rates come from in vitro assays with membrane preparations, and these rates may be significantly different from in vivo rates. CheR and CheB are localized to the compact chemoreceptor cluster so their activities may be strongly affected by their enhanced local concentration and the close proximity of other proteins. In fact, it can be argued that by titrating the adaptation rates against other parameters of the pathway, we are likely to arrive at more realistic values. When a simulation such as this becomes sufficiently data-rich, it provides a test of consistency between multiple experimental measurements, which are often made at disparate times and in different laboratories.

The increased activities of CheR and CheB had an influence on not only the characteristics of the impulse response but also the ability of the cells to accumulate in a gradient (see Figure 5). In fact, a link between these two aspects of the *E. coli* chemotactic response was noted previously. In theoretical work by Clark and Grant [18], the authors showed that the independent criteria of movement up a chemotactic gradient and accumulation at peaks of chemoattractant are in conflict. They

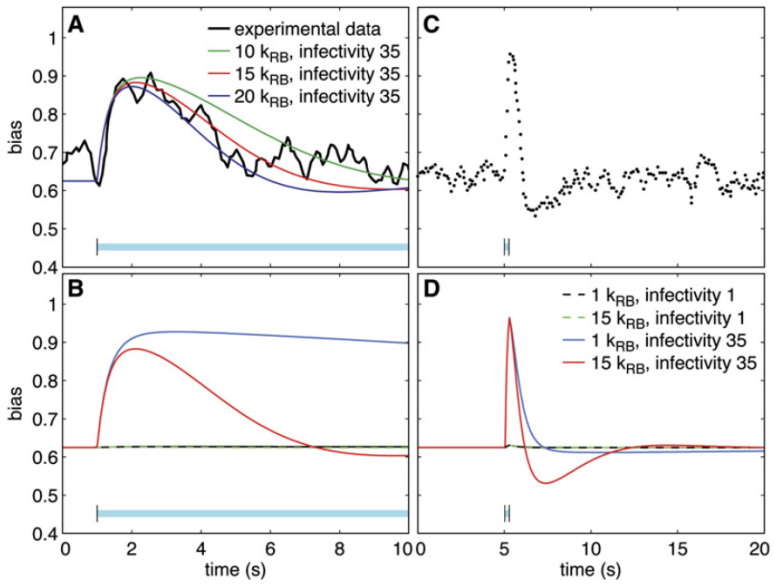

Figure 4. Response to Steps and Pulses of Aspartate

(A) Step increase of 15 nM aspartate. Simulations were run with different coordinate rates of methylation and demethylation ($k_{R,B}$) and fixed infectivity. The experimental step response is replotted from the data of Segall et al. [3]. Vertical bars and cyan shading indicate the presence of aspartate.

(B) Same as (A) but with different levels of infectivity (see [D] for legend).

(C) Experimental impulse response replotted from the data of Segall et al. [3].

(D) Results of BCT simulations of the response to a 0.25 s pulse of 0.8 M aspartate; cells with different coordinate rates of methylation and demethylation ($k_{R,B}$) and different levels of infectivity (gain) were used.

showed that composite optimization yields a response function that closely resembles the experimentally determined impulse response function, with a bias overshoot of equal magnitude. Their work clarifies why increasing the rate of adaptation not only produces a more accurate impulse response but also results in a superior accumulation at the peak of a gradient.

The experimental observation of bacterial chemotactic responses is technically difficult. Gradients of freely diffusing soluble molecules are inherently labile and liable to change over the periods of time needed for observing bacterial motility. Techniques that have been used in the past employed such devices as swarm plates and pipettes introduced into the bacterial culture. Bacteria have also been observed swimming in defined gradients established in glycerol solutions [19] or in microchannels between two stirred chambers [20]. Recently, microfluidic technology has been employed to create gradients of attractants and repellents, and the effects on free-swimming bacteria have been observed [21, 22]. A great deal has been learned from these experimental methods, but they all have their limitations. By comparison, our computer-based analyses are rapid and convenient. We can apply gradients of any shape and perfect stability and measure bacterial responses, both behavioral as well as biochemical, to these gradients, with any desired accuracy and sensitivity. Because our simulated bacteria contain a replica of the signal transduction pathway found in real bacteria and, within the limits already noted, perform in a closely similar fashion, we feel justified in treating them as experimental objects in their own right. They serve as surrogate bacteria in tests that would be difficult, if not impossible, to perform experimentally.

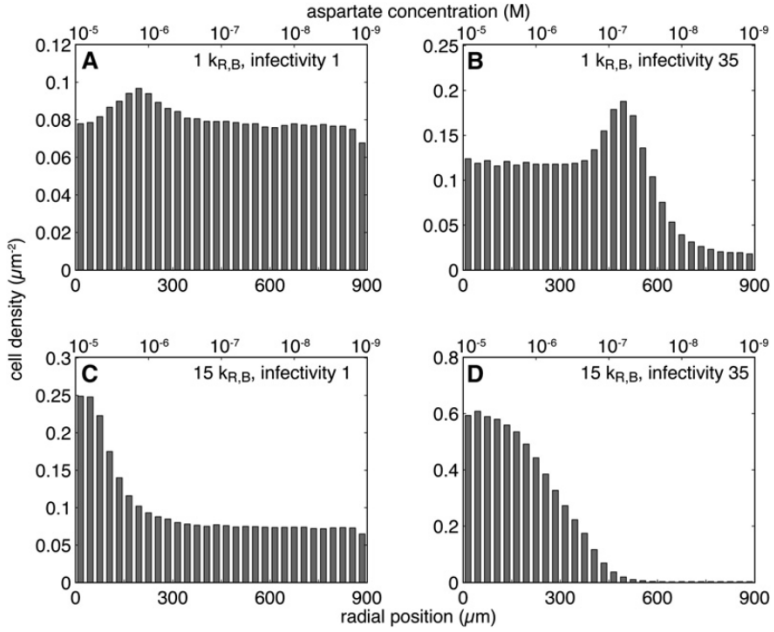

Figure 5. Distribution of *E. pluribus* in a Radial Gradient

One thousand simulated bacteria were placed at random in a circular arena of radius 900 μm. The arena contained an exponential gradient of aspartate, from 10^{-5} M in the center to 10^{-9} M on the perimeter. After 100 s so that a steady-state distribution could be reached, the positions of bacteria were recorded at 2 s intervals for the next 1000 s and pooled. Histograms show the average density of bacteria in 30 radial sectors.

(A) Default bacteria with infectivity of 1.

(B) Default bacteria with infectivity of 35.

(C) Adaptation-enhanced strain with the catalytic activities of CheR and CheB increased 15-fold greater than rates used in the unmodified BCT program and infectivity of 1.

(D) Same as (C) but with infectivity of 35.

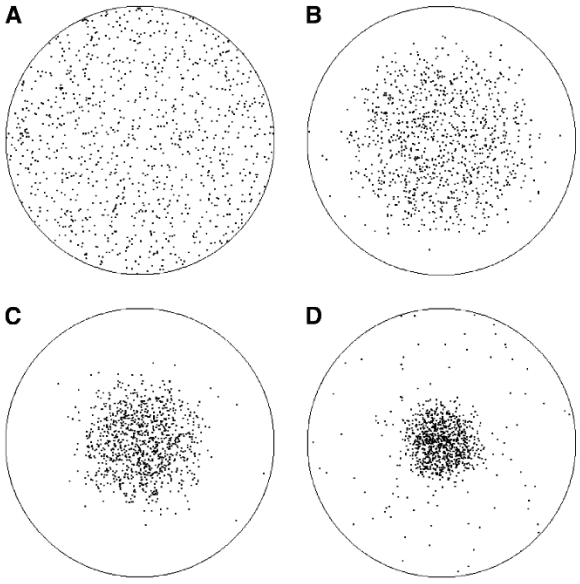

Figure 6. Accumulation in Different Gradients

The positions of 1000 *E. pluribus* cells were recorded after 1200 s. In every case, a strain with the catalytic rates of CheR and CheB increased 15-fold, and infectivity of 35 was used.

(A) No gradient.

(B) Exponential gradient from 10^{-4} M aspartate in the center to 10^{-8} M on the perimeter.

(C) Gradient from 10^{-5} M to 10^{-9} M.

(D) Gradient from 10^{-6} M to 10^{-10} M.

To illustrate the superior analytical possibilities inherent in a computer-based approach, we measured the distribution of bias and level of methylation in populations of cells. This revealed systematic changes, which would have been difficult to measure experimentally, at different points along a gradient. The value of such an analysis was highlighted in the case of the distinctive "volcano" distribution we encountered in certain gradients. We saw that cells in steep radial gradients of attractant accumulate at highest density in a ring situated at intermediate concentrations and show a lower plateau density closer to the center (see Figure 7 and Figure S1). This is in accordance with the observation made by Julius Adler in 1973 of the behavior of bacteria in a capillary assay, in which an attractant diffuses from the mouth of the capillary and creates a gradient: "A cloud of bacteria does form away from the mouth of the capillary whenever the attractant is present at concentrations that are effective for chemotaxis" [23]. On further analysis, we found that the highest incidence of tumbling (lowest bias) coincided with the rim of the volcano (position of highest cell density), whereas methylation levels reached a steady maximum value in the volcano crater (Figure 7B). Our interpretation is that cells attracted to the gradient swim across the region of highest concentration at its center until they reach a sufficiently low concentration to cause a tumble. At this point (corresponding to the peak of density), they change direction randomly until by chance they set off again across the peak region. Evidently in the future we will be able to analyze other more complex situations. These will include investigations of individuality in the population [12, 24] and the response to mixed gradients of different shapes.

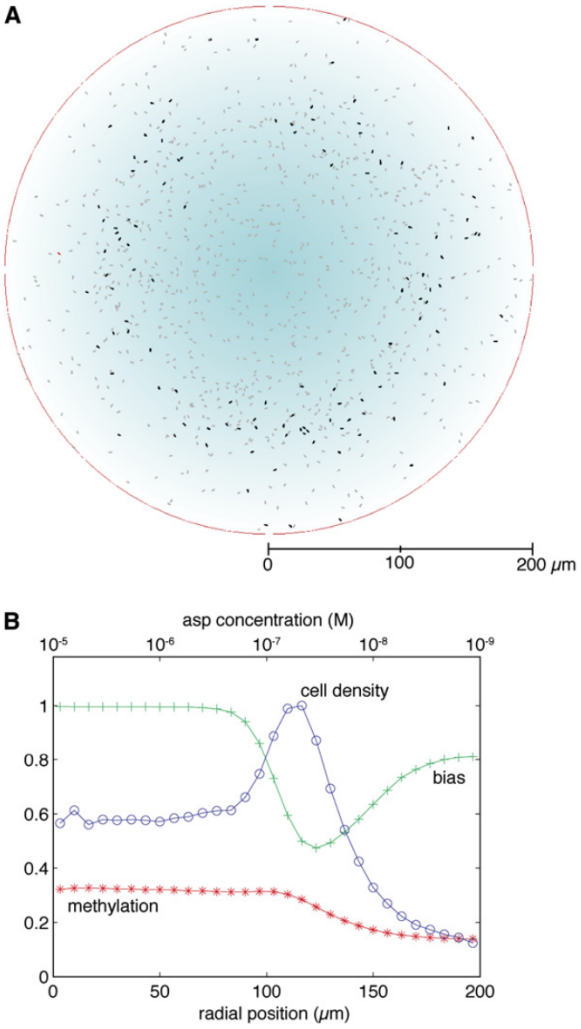

Figure 7. Depiction and Analysis of the "Volcano Effect"

(A) A screen shot of 1000 *E. pluribus* cells distributed in a radial gradient of aspartate (decreasing exponentially from 10^{-5} M in the center to 10^{-9} M at the perimeter) and allowed to come to a dynamic equilibrium. The radius of the gradient was reduced to 200 μm so that individual cells could be displayed to scale. Cells undergoing a tumble are shown in black; cells in a run are in gray. Notice the ring of tumbling cells.

(B) The same simulation depicted in (A) was averaged over 20 min so that average values could be calculated. Normalized cell density is represented in blue, rotational bias is in green, and methylation level is in red. In each case, values were summed within radial segments.

Experimental Procedures

The BCT Program

Early versions of the BCT program (Bacterial ChemoTaxis) are described in previous publications [10, 25]. The current version is available for download from our web site (http://www.pdn.cam.ac.uk/comp-cell/BCT.html). In brief, the program models the cascade of protein-based reactions between the binding of aspartate to transmembrane chemotaxis receptors (the input) and the rotational switching of flagellar motors (the output) as a series of about 90 ordinary differential equations. These include binding reactions (such as between an attractant molecule and the receptor or between the receptor and CheA) and catalytic reactions (such as phosphorylation of CheA, methylation of the receptor, and the like). On initiation, the program performs a set of "prebind" reactions in which receptors, CheW, and CheA associate to form a functional ternary

complex [10]. Subsequent simulation cycles then employ this assembled complex so that phosphorylation and other signaling reactions can be performed.

Experimental Data

Rates and concentrations used in the BCT program are based on quantitative data reported in the large published literature. Parameter values (seven concentrations and 14 independent rate constants) and their sources are listed as part of the program and are available from http://www.pdn.cam.ac.uk/compcell/Rates.html (see Tables S1 and S2 in the Supplemental Data available with this article online for protein concentrations and kinetic data used in this work). In a few cases, we have found it necessary to adjust these values: The binding affinities of CheW to the serine receptor Tsr and CheA are larger than reported values so that overproduction mutants are faithfully reproduced [10]; adjustment of the catalytic rates of CheR and CheB are discussed in this paper.

Program Input and Output

Inputs to the BCT program include the copy number per cell of each of seven chemotaxis proteins and the extracellular concentration of aspartate. The output comprises a list of concentrations of 38 signaling species; this list is updated every 20 ms. The program also uses the concentration of CheYp to calculate the swimming *bias*, defined as the fraction of time that a cell spends in smooth swimming (caused by counterclockwise rotation of the flagellar motors). For any given (average) run duration, the bias then determines the probability that an individual cell will undergo a tumble in the next time step. We also incorporated a small random change in direction during a run (called a "shimmy") to simulate thermal drift. This was adjusted so that a correlation length of about 10 μm could be produced, as observed experimentally with swimming cells [9].

Supplemental Data

Supplemental Data include two tables and can be found with this article online at http://www.current-biology.com/cgi/content/full/17/1/12/DC1/.

Acknowledgments

We thank the anonymous reviewers for their constructive comments and suggestions, especially the reviewer who brought reference [23] to our attention. Thanks also to Mark DePristo and Aldo Faisal for valuable suggestions and the National Institutes of Health-National Institute of General Medical Sciences (GM64713).

Received: October 6, 2006
Revised: November 10, 2006
Accepted: November 13, 2006
Published: January 8, 2007

References

1. Berg, H.C. (2004). *E. coli* in Motion (New York: Springer-Verlag).
2. Wadhams, G.H., and Armitage, J.P. (2004). Making sense of it all: Bacterial chemotaxis. Nat. Rev. Mol. Cell Biol. *5*, 1024–1037.
3. Segall, J.E., Block, S.M., and Berg, H.C. (1986). Temporal comparisons in bacterial chemotaxis. Proc. Natl. Acad. Sci. USA *83*, 8987–8991.
4. Kim, C., Jackson, M., Lux, R., and Khan, S. (2001). Determinants of chemotactic signal amplification in *Escherichia coli*. J. Mol. Biol. *307*, 119–135.
5. Sourjik, V., and Berg, H.C. (2002). Receptor sensitivity in bacterial chemotaxis. Proc. Natl. Acad. Sci. USA *99*, 123–127.
6. Maddock, J.R., and Shapiro, L. (1993). Polar location of the chemoreceptor complex in the *Escherichia coli* cell. Science *259*, 1717–1723.
7. Sourjik, V. (2004). Receptor clustering and signal processing in *E. coli* chemotaxis. Trends Microbiol. *12*, 569–576.
8. Turner, L., Ryu, W.S., and Berg, H.C. (2000). Real-time imaging of fluorescent flagellar filaments. J. Bacteriol. *182*, 2793–2801.
9. Berg, H.C., and Brown, D.A. (1972). Chemotaxis in *Escherichia coli* analysed by three-dimensional tracking. Nature *239*, 500–504.
10. Bray, D., and Bourret, R.B. (1995). Computer analysis of the binding reactions leading to a transmembrane receptor-linked multiprotein complex involved in bacterial chemotaxis. Mol. Biol. Cell *6*, 1367–1380.
11. Levin, M.D., Morton-Firth, C.J., Abouhamad, W.N., Bourret, R.B., and Bray, D. (1998). Origins of individual swimming behavior in bacteria. Biophys. J. *74*, 175–181.
12. Spudich, J.L., and Koshland, D.E., Jr. (1976). Non-genetic individuality: Chance in the single cell. Nature *262*, 467–471.
13. Bray, D., Levin, M.D., and Morton-Firth, C.J. (1998). Receptor clustering as a cellular mechanism to control sensitivity. Nature *393*, 85–88.
14. Le Novère, N., and Shimizu, T.S. (2001). StochSim: Modelling of stochastic biomolecular processes. Bioinformatics *17*, 575–576.
15. Andrews, S.S., and Bray, D. (2004). Stochastic simulation of chemical reactions with spatial resolution and single molecule detail. Phys. Biol. *1*, 137–151.
16. Barnakov, A.N., Barnakova, L.A., and Hazelbauer, G.L. (2002). Allosteric enhancement of adaptational demethylation by a carboxyl-terminal sequence on chemoreceptors. J. Biol. Chem. *277*, 42151–42156.
17. Anand, G.S., Goudreau, P.N., and Stock, A.M. (1998). Activation of methylesterase CheB: Evidence of a dual role for the regulatory domain. Biochemistry *37*, 14038–14047.
18. Clark, D.A., and Grant, L.C. (2005). The bacterial chemotactic response reflects a compromise between transient and steady-state behavior. Proc. Natl. Acad. Sci. USA *102*, 9150–9155.
19. Dahlquist, F.W., Lovely, P., and Koshland, D.E., Jr. (1972). Quantitative analysis of bacterial migration in chemotaxis. Nat. New Biol. *236*, 120–123.
20. Berg, H.C., and Turner, L. (1990). Chemotaxis of bacteria in glass capillary arrays. *Escherichia coli*, motility, microchannel plate, and light scattering. Biophys. J. *58*, 913–930.
21. Mao, H., Cremer, P.S., and Manson, M.D. (2003). A sensitive, versatile microfluidic assay for bacterial chemotaxis. Proc. Natl. Acad. Sci. USA *100*, 5449–5454.
22. Diao, J., Young, L., Kim, S., Fogarty, E.A., Heilman, S.M., Zhou, P., Shuler, M.L., Wu, M., and DeLisa, M.P. (2006). A three-channel microfluidic device for generating static linear gradients and its application to the quantitative analysis of bacterial chemotaxis. Lab on a Chip *6*, 381–388.
23. Adler, J. (1973). A method for measuring chemotaxis and use of the method to determine optimum conditions for chemotaxis by *Escherichia coli*. J. Gen. Microbiol. *74*, 77–91.
24. Levin, M.D. (2004). Noise in gene expression as the source of non-genetic individuality in the chemotactic response of *Escherichia coli*. FEBS Lett. *550*, 135–138.
25. Bray, D., Bourret, R.B., and Simon, M.I. (1993). Computer simulation of the phosphorylation cascade controlling bacterial chemotaxis. Mol. Biol. Cell *4*, 469–482.
26. Parkinson, J.S., Ames, P., and Studdert, C.A. (2005). Collaborative signaling by bacterial chemoreceptors. Curr. Opin. Microbiol. *8*, 116–121.
27. Morton-Firth, C.J. (1998). Stochastic simulation of cell signalling pathways. PhD thesis, University of Cambridge, Cambridge.
28. Abouhamad, W.N., Bray, D., Schuster, M., Boesch, K.C., Silversmith, R.E., and Bourret, R.B. (1998). Computer-aided resolution of an experimental paradox in bacterial chemotaxis. J. Bacteriol. *180*, 3757–3764.